analytical chemistry

Article

Cite This: *Anal. Chem.* 2019, 91, 13794−13802

pubs.acs.org/ac

Automated High-Throughput Capillary Circular Dichroism and Intrinsic Fluorescence Spectroscopy for Rapid Determination of Protein Structure

Charles Moore-Kelly,[†,‡,⊥] John Welsh,[§] Alison Rodger,[∥] Tim R. Dafforn,[‡] and Owen R. T. Thomas*[,†]

[†]School of Chemical Engineering, and [‡]School of Biosciences, University of Birmingham, Edgbaston, B15 2TT, U.K.

[§]Pall Biotech, Southampton Road, Portsmouth, PO6 4BQ, U.K.

[∥]Department of Molecular Sciences, Macquarie University, Macquarie Park, Sydney, New South Wales 2109, Australia

Supporting Information

ABSTRACT: Assessing the physical stability of proteins is one of the most important challenges in the development, manufacture, and formulation of biotherapeutics. Here, we describe a method for combining and automating circular dichroism and intrinsic protein fluorescence spectroscopy. By robotically injecting samples from a 96-well plate into an optically compliant capillary flow cell, complementary information about the secondary and tertiary structural state of a protein can be collected in an unattended manner from considerably reduced volumes of sample compared to conventional techniques. We demonstrate the accuracy and reproducibility of this method. Furthermore, we show how structural screening can be used to monitor unfolding of proteins in two case studies using (i) a chaotropic denaturant (urea) and (ii) low-pH buffers used for monoclonal antibody (mAb) purification during Protein A chromatography.

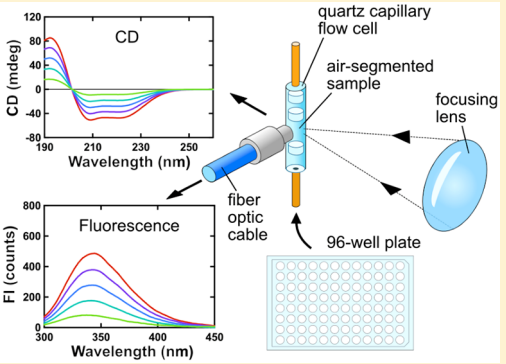

The majority of biologics are recombinant proteins produced by engineered microbial, plant, or animal cells, and processes for their manufacture rely on harmonious integration of a complex series of upstream and downstream operations.[1] The stringent requirements for proving that biotherapeutic protein products are correctly folded into the active three-dimensional (3D) structure is a vital concern of the biopharma industry. Proteins, especially large complex human proteins, exhibit a propensity to unfold and aggregate in response to often quite small changes in the process environment.[2,3] Loss of structural integrity is a recognized factor in reducing a drug's therapeutic efficacy and invoking immune responses in patients.[4,5]

The considerable number of factors that influence biotherapeutic quality attributes has contributed to a series of risk-based initiatives governing their manufacture.[6] These measures aim to safeguard product consistency, quality, and purity by ensuring that the manufacturing process remains substantially the same over time. Important among these is the Food and Drug Administration's guidance on Process Analytical Technology (PAT) within the pharmaceutical sector.[7−9] In the case of biotherapeutic protein targets, where maintenance of the correct 3D structure is essential for drug efficacy, improved understanding of the impact of processing environments relies, in large part, on the development of robust high-throughput analytical techniques capable of effectively monitoring a given protein's structural state at all stages during processing and formulation.[10]

Circular dichroism (CD) and intrinsic fluorescence are sensitive, nondestructive biophysical techniques employed for studying changes in the solution-state conformation of proteins.[11,12] CD is a spectroscopic technique that measures the differential absorption of left- and right-handed circularly polarized light. Asymmetric absorption of the peptide backbone in the far-UV region provides an excellent means of measuring changes in the total secondary structure of a protein, while absorption in the near-UV region arising from aromatic amino acids provides a good indicator of tertiary structure changes. Intrinsic protein fluorescence is a complementary technique that provides information on the state of protein structure from changes in the local environment of aromatic amino acid residues.[13−17]

An existing challenge with using CD and fluorescence together for routine structural screening is that instruments are not configured for use in an industrial setting, where speed and autonomy are paramount. Conventionally, far-UV CD is carried out in quartz cuvettes with a path length of 0.1 cm, requiring ∼200 μL protein samples of 0.1−0.2 mg/mL.[11] Unless a CD spectrometer has been specifically adapted with a dedicated fluorescence detector, fluorescence spectra are gathered using a separate instrument in a different cuvette. As both protein sample and buffer spectra must be collected

Received: July 18, 2019
Accepted: October 4, 2019
Published: October 4, 2019

DOI: 10.1021/acs.analchem.9b03259
Anal. Chem. 2019, 91, 13794−13802

(ideally in the same cuvette for CD) with cleaning between measurements, performing spectral analyses on many samples can be time-consuming. Further, the optical constraints of CD render the use of traditional plate reader type formats difficult, motivating past approaches to increase sample throughput either by increasing the number of cuvettes using a carousel holder[18] or employing a liquid handling robot to load a fixed-position, square-faced cuvette.[19]

A different approach to increasing sample throughput has been taken in this work, inspired in part by the pioneering work of Synovec and Yeung,[20,21] and in particular, building on an earlier study by Waldron et al.[22] who introduced an ultralow volume system for CD comprising an extruded quartz capillary as the optical cell (replacing the standard quartz cuvette) and modified optical configuration. Specifically, we detail the systematic development and validation of an automated high-throughput capillary-based CD/fluorescence (ht-caCD/F) measurement system and demonstrate its utility as a PAT tool for bioprocess development work. First, we describe the components of the measurement system, placing special emphasis on pairing the optically transparent flow cell with an optical arrangement that maximizes low-wavelength performance. Second, we show how sample delivery was optimized to allow highly efficient transfer of samples as small as 40 μL containing just 4 μg of protein. Finally, we employ the ht-caCD/F system as a PAT tool for (i) monitoring conformational changes of bovine serum albumin (BSA) and a monoclonal antibody (mAb) under chemical denaturing conditions and (ii) measuring changes to the structure of the mAb on exposure to 24 different buffers spanning pHs of 2.2−8.05.

EXPERIMENTAL SECTION

Materials. The quartz capillary (3.5 mm o.d, 1.20 mm i.d) and PEEK tubing (1.59 mm o.d., 0.25 mm i.d.) employed for construction of the flow cell were purchased from Enterprise-Q (Manchester, Lancs, U.K.) and BGB Analytik Vertrieb GmbH (Rheinfelden, Germany), respectively. Both the uncoated UV fused-silica double convex lens (25 mm diameter, 50 mm effective focal length; cat. no. 48-294) used to focus the light beam in front of the flow cell and focusing lens mount were provided by Edmund Optics Ltd. (Nether Poppleton, York, Yorks, U.K.). Corning 96-well NBS microplates were acquired from Corning Life Sciences B.V. (Amsterdam, The Netherlands), and the bioinert Rheodyne model 9010 six-port injector was supplied by Merck KgaA (Darmstadt, Germany). The purified humanized IgG1 mAb used in this work targets the HER2 receptor and was provided by Pall Biotech (Portsmouth, Hants, U.K.) at a stock concentration of 10 mg/mL in 10 mM sodium phosphate pH 7.1 buffer. Prior to sample preparation, 0.3 mL aliquots of stock mAb were exchanged into water by means of size exclusion chromatography using PD MiniTrap G-10 columns (GE Healthcare, Uppsala, Sweden), and mAb concentration was determined in a spectrophotometer assuming $A^{1\%}_{279nm}$ = 15.0. Bovine serum albumin Cohn fraction V (fatty acid free, low endotoxin, lyophilized powder; $A^{1\%}_{279nm}$ = 6.67) and chemicals, glycine (≥98.5%), anhydrous sodium acetate (≥99.0%), and (1*S*)-(+)-10-camphorsulfonic acid (CSA) ammonium salt, were obtained from Merck KgaA (Darmstadt, Germany). Glacial acetic acid (≥99.7%), hydrochloric acid (∼37%), urea (≥99.5%, Electran molecular biology grade), sodium dihydrogen orthophosphate dihydrate (≥99.0%), and anhydrous disodium hydrogen orthophosphate (≥99.5%) were supplied by Fisher Scientific U.K. (Loughborough, Leics, U.K.). Citric acid monohydrate (≥99.7%) and trisodium citrate dihydrate (≥99.0%) were acquired from VWR International (Leighton Buzzard, Beds, U.K.), and Hellmanex II special cleaning concentrate was from Hellma GmbH & Co. KG (Müllheim, Germany). All other materials were obtained from Merck KgaA (Darmstadt, Germany), and all solutions were prepared using deionized water (resistivity 15.0 MΩ·cm at 22 °C) purified by a PURELAB Option-R Ultra water purification system (ELGA LabWater, High Wycombe, U.K.).

Instrument Overview. Figure 1A shows a schematic representation of the automated sampling system developed using parts from a high-performance liquid chromatography (HPLC) system plus an extruded quartz capillary cut from a length supplied by Enterprise-Q. It comprises a modified autosampler (Jasco AS-2055) and HPLC pump (Jasco PU-1580) configured to inject protein samples into a quartz capillary flow cell held in the beam path of a Jasco J-1500 CD spectrometer (Jasco U.K. Ltd., Great Dunmow, Essex, U.K.) which is focused down to the 1 mm wide capillary window of the sample holder. During sample loading, sample is drawn from a 96-well plate using a three-axis robotic needle, and then transferred to a holding loop for injection. A mobile phase of deionized water transfers sample to the capillary, and on reaching the flow cell, flow is stopped. The CD spectrometer and fluorescence detector are then electronically triggered to analyze the sample. Fluorescence spectra are recorded using an Ocean Optics HR2000+ CCD array detector with a fiber-optic cable attachment (Ocean Optics, Largo, FL, U.S.A.). CD and absorbance spectra are simultaneously collected thereafter by the CD spectrometer.

Flow Cell Design. A flow cell was constructed by carefully tapering the ends of two pieces of PEEK tubing (60 and 2 cm) with a scalpel to allow their insertion (∼5 mm deep) into either end of a 3 cm length of quartz capillary (Figure 1B). Araldite rapid two-part epoxy glue was applied to the joints, which were then heated over a Bunsen flame to create tight seals. The long PEEK delivery tube of the flow cell was attached directly to the column outlet of the autosampler's six-way valve (Figure 1A) in order to reduce the volume from injection valve to capillary down to ∼30 μL, and flexible PTFE waste tubing was connected to the short PEEK exit tube. A 3D-printed capillary mounting (Figure 1, parts B and C) designed using AutoCAD software (AutoDesk Inc., San Rafael, CA, U.S.A.) was employed to securely fix the capillary within the beam and immediately in front of the instrument's photomultiplier tube (Figure 1A). The capillary mounting features 1 mm wide apertures at the entrance and exit faces of the capillary (Figure 1, parts B and C) to mask the capillary edges from incoming light, thereby ensuring that light reaching the detector has passed through, and not around, the contained sample. An opening at 90° to the incident beam was made in the capillary mounting (Figure 1, parts A and C) in order to accommodate the SMA-905 attachment of the fiber-optic cable for detecting fluorescence, and a 2.5 cm quartz biconvex lens of 5.0 cm focal length was fitted to the sample stage of the spectrometer to focus light onto the front face of the capillary and enhance spectral resolution (Figure 1, parts A and C).

Sample Handling. To eliminate potential sample adsorption within the flow path, the stainless-steel needle, transfer tube, and holding loop of the autosampler were all replaced with PEEK tubing. Sample dilution on delivery was

DOI: 10.1021/acs.analchem.9b03259
Anal. Chem. 2019, 91, 13794−13802

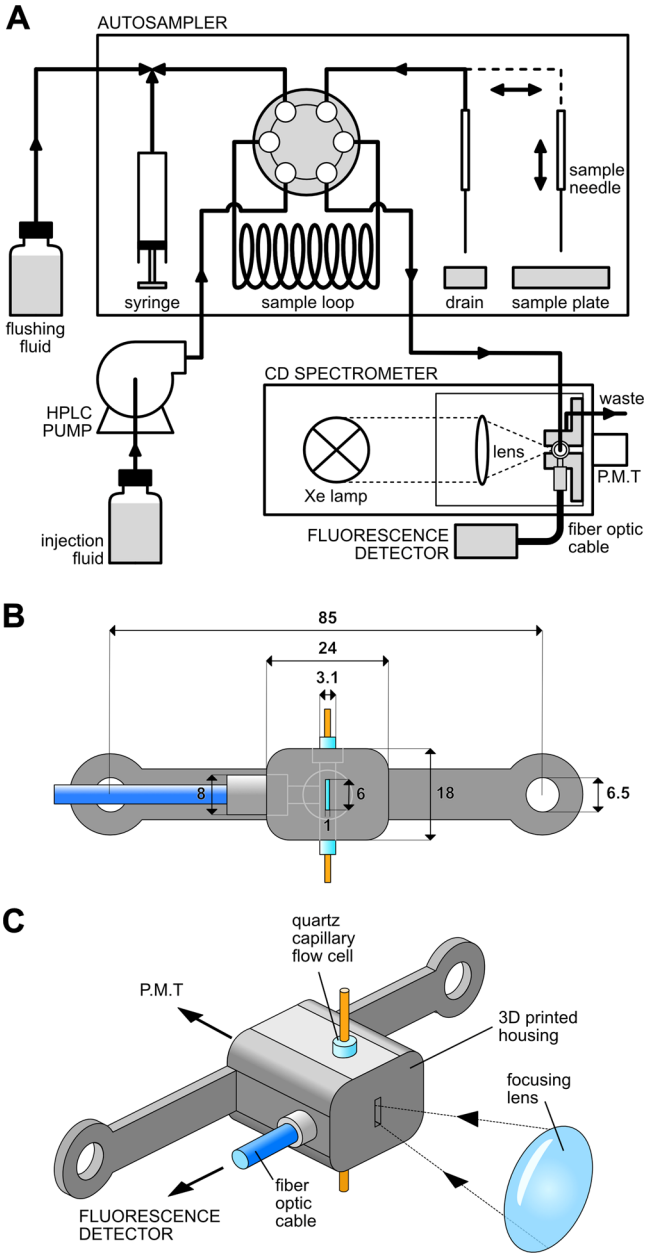

Figure 1. (A) Schematic diagram of the automated circular dichroism and fluorescence system. The autosampler retrieves sample from a 96-well plate, and sample is injected to the flow cell. Sample injection is controlled by a pump profile programmed on the HPLC pump. (B) Front view of flow cell with dimensions. (C) Annotated isometric view of the flow cell and focusing lens.

minimized by adjusting the autosampler's aspiration settings to separate the sample from the flanking mobile phase by sandwiching between two air bubbles ("double" air-segmented delivery), the sizes of which were adjusted by altering the volume of air drawn before and after the sample. Further, to limit potential dilution of analytes by residual mobile fluid on the flow path walls, the use of an additional air bubble encased sacrificial wash sample traveling immediately ahead of the bona fide sample ("triple" air-segmented delivery) was also explored; schematic illustration is provided in Figure S1. For information on the settings employed for two and three air bubble segmented sample delivery, refer to Table S1.

The pump was programmed to load samples at a flow rate of 5.5 μL/s, and the timings were set so that flow stopped immediately following full sample entry into the capillary (Table S2). After analysis, samples were ejected from the flow cell at a flow rate of 16.7 μL/s. The autosampler was programmed to perform five consecutive flushes of the needle and transfer tubing after each injection. To avoid cross-contamination from sample carryover, a solution of 2% (v/v) Hellmanex II was loaded after each protein sample. Buffer blank, protein sample, and cleaning agent elements were arranged in repetitive pattern across a 96-well plate, and the plate was tightly sealed with plastic wrap to prevent evaporation of sample during measurement time.

Optical Measurement. The CD spectrometer was used to collect CD and absorption spectra and provide a source of excitation light for fluorescence detection. Depending on the nature of individual experiments, CD data were collected in time course, step scanning, or continuous scanning modes; the settings used in each case are given in the accompanying figure legends. Fluorescence excitation was carried out with a wavelength of 290 nm, bandwidth of 9 nm, and digital integration time (DIT) of 3 s (unless otherwise stated), and emission spectra were collected at 90° with a 25 cm length of 1 mm core diameter fiber-optic cable to take the light to the detector. The path length of the capillary flow cell (1.18 mm) was determined by comparing the amplitude of the high-wavelength 292 nm peak of a 1 mg/mL solution of CSA in deionized water with that obtained using the 1 mm standard cuvette.

Automation. The HPLC pump, CD spectrometer, and fluorescence detector were electronically interfaced in order to synchronize scanning routines with sample injection (Figure S2). Two event channels were assigned within the HPLC pump profile to provide separate triggering control for the CD and fluorescence spectrometers. A Raspberry Pi model B+ (Raspberry Pi Foundation, Cambridge, Cambs, U.K.) was used as a central hub to receive event channel signals from the HPLC pump and initiate spectrometers. A potential difference of 3.3 V was applied to the two-event channel termini of the HPLC pump, so events could be detected via two pull-down input general-purpose input/output (GPIO) pins on the Raspberry Pi. A program written in Python version 3.5.0 (https://www.python.org/downloads/release/python-350/) was used to process incoming event channel signals and relay them to external trigger pins of the spectrometers via output GPIO pins (Table S3).

The CCD array fluorescence detector was grounded via pin 5 of its input/output terminal, and the device was triggered to record multiple spectra by applying a 3.3 V pulse to pin 10, which could be programmed to last the desired integration time within the program running on the Raspberry Pi (Table S3). Fluorescence spectra were recorded and saved during the signaling interval using the "software input" mode of the accompanying Ocean Optics SpectraSuite software.

Triggering of the CD spectrometer was controlled via a relay switch circuit, comprising an NPN transistor (S8050) and relay switch (SRD-05VDC-SL-C) (SunFounder starter kit V2.0 for Arduino). A 3.3 V output signal from a Raspberry Pi GPIO to the transistor base terminus was used to close the circuit between positive and negative trigger pins of the CD spectrometer and initiate the macro sequence. Macro commands for the initiation of CD and fluorescence scanning routines (Table S2) were written in Jasco Spectra Manager II.

DOI: 10.1021/acs.analchem.9b03259
Anal. Chem. 2019, 91, 13794−13802

Upon the CD spectrometer receiving an external signal, macro commands open the beam shutter to expose the sample to excitation light for fluorescence, and an event signal is sent to the CCD array detector to trigger the collection of fluorescence spectra. Once fluorescence spectra have been collected, the shutter is closed, and the monochromator then resets to carry out CD scanning routines. Macro commands were enclosed in a loop function to allow the reiteration of this program with the loading of each new sample. A program written in Python 3.5.0 was used to accumulate and average fluorescence.txt files following data collection (Table S3).

RESULTS AND DISCUSSION

Design and Calibration of the Flow Cell. In contrast to conventional flat-walled CD sample chambers, the use of curved walls of the capillary might be expected to convey some optical distortion. To test the capillary-based CD/fluorescence (ht-caCD/F) measurement system (Figure 1) for its suitability in automated bioprocess development work, calibration data were collected from samples of 1 mg/mL CSA (Figure 2A) and 0.1 mg/mL BSA (Figure 2B). CD spectra were recorded using the capillary flow cell "with" and "without" the focusing lens, and optical quality was compared to spectra collected in a standard 1 mm path length quartz cuvette. For ease of comparison, the 1 mm cuvette ellipticity data were scaled to a 1.18 mm path length (i.e., multiplied by 1.18).

The data show that CD spectra from the capillary closely approached the quality achieved with a standard cuvette (Figure 2). The acquired spectra highlight the important role of the focusing lens in significantly improving light flux through the sample chamber [represented by a lower high-tension (HT) voltage; Figure 2, parts C and D], thereby reducing spectral noise across the entire wavelength range (185−270 nm). The two-point CSA calibration ratios[23] were −2.00 for the "capillary flow cell + lens" setup; cf. −2.03 for the cuvette (Figure 2A). Small deviations (more noticeable for BSA; Figure 2B) only become apparent below 200 nm due to increased HT voltage (i.e., lower photon flux) at lower wavelengths.

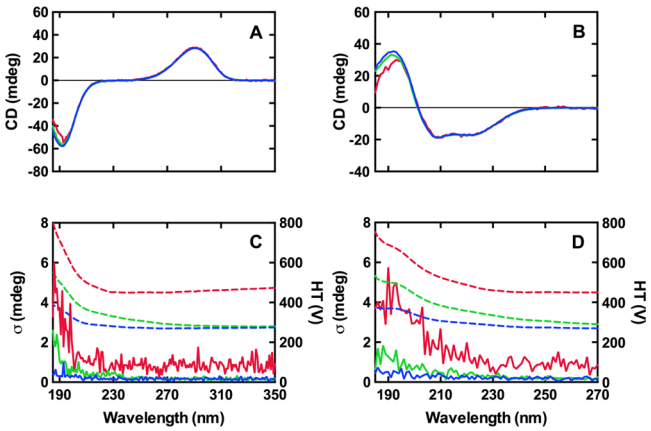

Figure 2. Optical comparisons of a quartz capillary flow cell (with and without focusing lens) and a standard quartz cuvette conducted using (A) 1 mg/mL CSA and (B) 0.1 mg/mL BSA. Spectra were measured in step scan mode (bandwidth = 1 nm, and DIT = 1 s). Individual CD spectra and HT voltage traces from six consecutive scans were averaged. Spectral "noise" plots (standard deviation in CD, σ vs wavelength) corresponding to the averaged CD spectra in panels A and B are shown in panels C and D, respectively. The standard cuvette data were multiplied by 1.18 for direct comparison with the capillary data. Key: cuvette (blue lines); capillary (red lines); capillary with focusing lens (green lines); CD spectra and spectral noise (solid lines); HT (dashed lines).

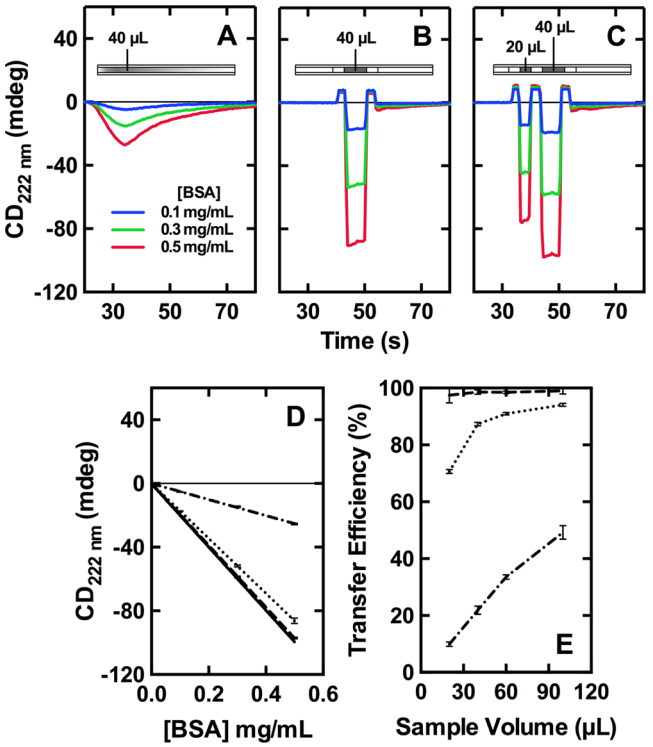

Figure 3. Comparison of direct and air-segmented sample delivery to the capillary flow cell. "CD_{222nm} vs time" flow profiles arising from delivery of 40 μL of 0.1, 0.3, and 0.5 mg/mL BSA to the flow cell at a flow rate of 5.5 μL/s by (A) direct injection into the carrying stream, (B) double air (20 μL first leading air/40 μL sample/20 μL trailing air), and (C) triple air (20 μL first leading air/20 μL sacrificial wash sample/20 μL second leading air/40 μL sample/20 μL trailing air) segmented injection. Measurements were made in time course measurement mode (bandwidth = 2 nm; measurement interval = 0.5 s; DIT = 0.5 s). Three injections of each sample were performed, and averaged profiles are shown. (D) "Maximum CD_{222nm} vs BSA loading concentration" and (E) "transfer efficiency vs sample volume" (0.1 mg/mL BSA was used) for direct (dash-dotted line), double air-segmented (dotted line), and triple air-segmented (dashed line) sample injections into the capillary flow cell and normalized static measurement in the standard cuvette (solid line). The error bars in panels D and E derive from three repeated injections at each concentration.

Secondary structure deconvolution performed on the derived BSA spectra using SELCON3[24] and CDSSTR[25] algorithms (reference data set 4, 240−190 nm) gave very similar average α-helix contents of 63 ± 3% for the cuvette cf. 60 ± 4% for the "capillary + lens" arrangement, demonstrating that the use of a capillary sample chamber had no significant impact on structural interpretation.

Sample delivery was optimized in experiments employing BSA injected independently at three different concentrations (0.1, 0.3, and 0.5 mg/mL in 10 mM sodium phosphate buffer, pH 7.4) through the flow cell at a flow rate of 5.5 μL/s, without stopping flow (Figure 3). The CD spectrometer was set to record at a wavelength of 222 nm, at which BSA displays a strongly negative elliptical signal. Resulting "CD_{222nm} vs time"

DOI: 10.1021/acs.analchem.9b03259
Anal. Chem. 2019, 91, 13794−13802

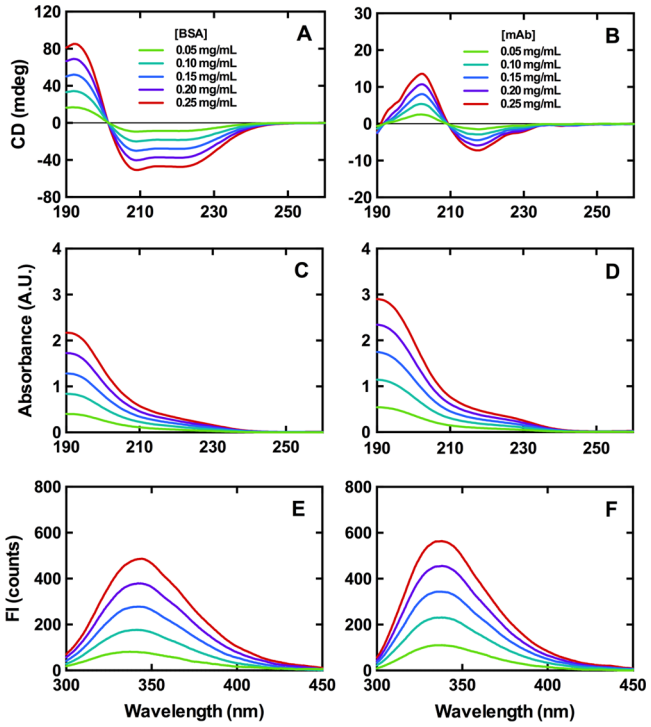

Figure 4. CD (A and B), UV absorption (C and D), and fluorescence (E and F) spectra of BSA (left) and mAb (right) acquired with the ht-caCD/F system. Triple air-segmented delivery was employed to inject 40 μL samples of BSA (in 10 mM sodium phosphate, pH 7.4) and mAb (in 10 mM sodium phosphate and 154 mM NaF, pH 7.1) loaded at concentrations of 0.05−0.25 mg/mL. Each sample was loaded three times at a flow rate of 5.5 μL/s, and the averaged spectra are shown. CD spectra (A and B) were collected in continuous scan mode with the following parameters: bandwidth = 2 nm; scan speed = 100 nm/min; DIT = 1 s; averaging over five scans per sample. Fluorescence spectra (E and F) were averaged over 14 accumulated scans per sample (DIT = 3 s).

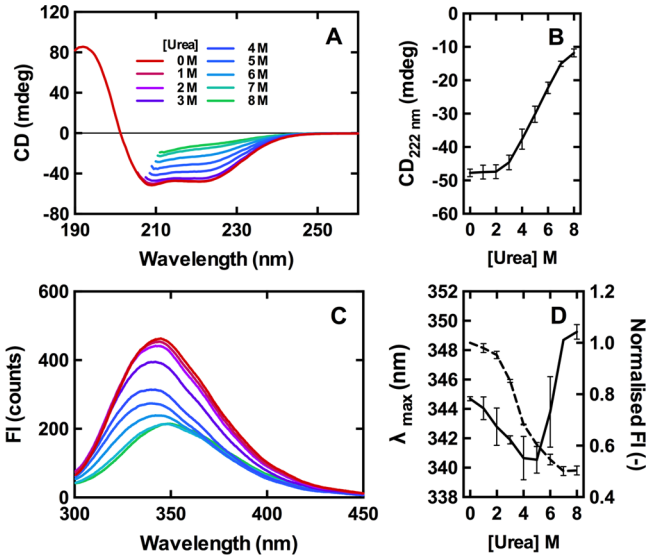

Figure 5. Case study 1a: using ht-caCD/F to interrogate protein unfolding. BSA (2.25 mg/mL) in 10 mM sodium phosphate pH 7.4 was diluted 9-fold with varying amounts of urea (in the same buffer) and mixed (1 h, room temperature) to give samples with final BSA and urea concentrations of 0.25 mg/mL and 0−8 M, respectively. Triple air-segmented delivery was employed to inject 40 μL samples. Each sample was loaded twice, and obtained spectra were averaged. (A) CD spectra were collected in continuous scan mode with the following parameters: bandwidth = 2 nm; scan speed = 100 nm/min; DIT = 1 s; averaging over five accumulated scans per sample. (B) CD_{222nm} vs urea concentration. (C) Fluorescence spectra were averaged over 14 accumulated scans per sample (DIT = 3 s). (D) λ_{max} (solid line) and normalized fluorescence intensity (dotted line) vs urea concentration. The error bars correspond to the standard deviation of two independent measurements.

profiles for three different sample injection modes are shown in Figure 3A−C. The maximum CD_{222nm} values derived from these are plotted against the BSA loading concentration (Figure 3D), and the impact of sample volume on transfer efficiency is also shown (Figure 3E).

Direct injection of 40 μL samples into the mobile carrier phase (Figure 3A) resulted in nearly 5-fold dilution (Figure 3D) due to zone broadening upon transfer to the flow cell. To limit sample diffusion in the carrying fluid, the sample aspiration settings of the autosampler were modified to introduce discrete volumes of air either side of the sample, i.e., one immediately in front, the other immediately behind. The bubbles of air appear in the flow profiles (Figure 3, parts B and C) as concentration-independent positive ellipticity signals on either side of the protein sample, arising as a result of distortion to the path of light passing through an air-filled capillary.

The effectiveness of air bubble segmented sample injection in eradicating the gross sample dilution by the mobile phase cf. direct injection (Figure 3A) is demonstrated in Figure 3B−E. The delivery of a 40 μL sample sandwiched between two 20 μL air bubbles, i.e., "double air" segmented injection (Figure 3B), increased the "carried sample" concentration 4-fold to 87.3 ± 0.6% of the theoretical maximum ellipticity, i.e., assuming no dilution of sample (Figure 3D). Variation in segmenting air bubble size between 5 and 30 μL revealed some sample bleed with the smallest bubbles tested (5 μL), but the carrying concentration of sample protein (measured as CD_{222nm}) appeared independent of bubble volume over the examined range (Figure S3).

The efficiency of sample carriage could be improved yet further (Figure 3C) to 98.6 ± 0.8% of the theoretical ε_{max} (Figure 3D) by introducing an air bubble segmented "sacrificial sample" (20 μL) immediately ahead of the "measured" sample (40 μL). This sacrificial sample served to "buffer" the impact of dilution on the main analyte caused by residual mobile phase in the flow path or capillary. An important advantage of this "triple" air-segmented sample delivery is that it permits delivery of much smaller sample volumes at high transfer efficiency (Figure 3E). For example, 20 and 40 μL samples of 0.1 mg/mL BSA can be delivered at efficiencies of 97.5 ± 2.7% and 98.6 ± 0.8%, respectively, cf. 70.7% and 87.3% for double air-segmented and just 9.9% and 21.9% for direct injection modes. In each instance, the independent delivery of protein to the flow cell showed highly reproducible flow profiles and concentrations.

Collection of full CD and fluorescence spectra using automated triple air-segmented sample delivery was subsequently evaluated by loading varying concentrations of BSA and mAb in the ht-caCD/F system and pausing flow for scanning routines. Specifically, this entailed preparing multiwell plates containing repeated sequences of buffer blank, protein sample, and 2% (v/v) Hellmanex cleaning solution and automatically collecting CD and fluorescence spectra from 40 μL samples loaded independently three times. Parts A, C,

DOI: 10.1021/acs.analchem.9b03259
Anal. Chem. 2019, 91, 13794−13802

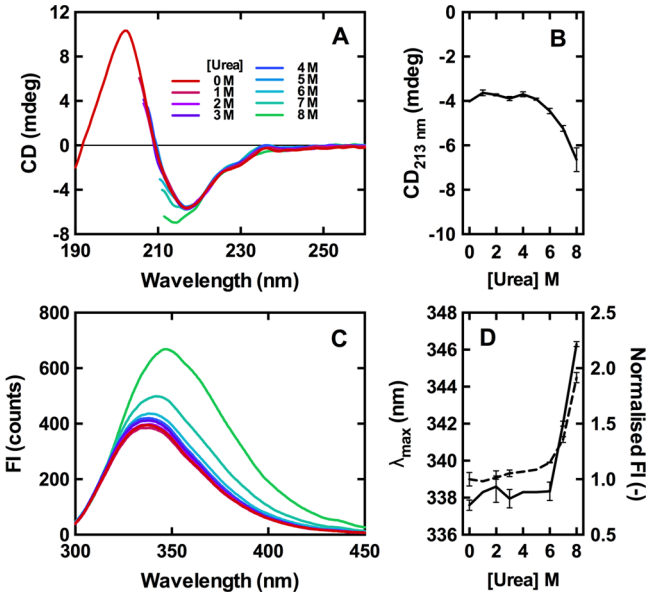

Figure 6. Case study 1b: using ht-caCD/F to interrogate protein unfolding. mAb (1.80 mg/mL) in 10 mM sodium phosphate pH 7.1 was diluted 9-fold with varying amounts of urea (in the same buffer) and mixed (1 h, room temperature) to give samples with final mAb and urea concentrations of 0.20 mg/mL and 0−8 M, respectively. Triple air-segmented delivery was employed to inject 40 μL samples. Each sample was loaded twice, and obtained spectra were averaged. (A) CD spectra were collected in continuous scan mode with the following parameters: bandwidth = 2 nm; scan speed = 100 nm/min; DIT = 1 s; averaging over five accumulated scans per sample. (B) Fluorescence spectra were averaged over 14 accumulated scans per sample (DIT = 3 s). (C) CD_{222nm} vs urea concentration. (D) λ_{max} (solid line) and normalized fluorescence intensity (dotted line) vs urea concentration. The error bars correspond to the standard deviation of two independent measurements.

and E of Figure 4 show the CD, absorption, and fluorescence spectra obtained for five different concentrations of BSA (0.05−0.25 mg/mL) in 10 mM sodium phosphate buffer, pH 7.4, averaged across three independent repeat injections. The CD spectra (Figure 4A) display the characteristic shape expected for BSA (RCSB PDB ID 3V03), an α-helical protein with intense negative maxima at 222 and 208 nm arising from the n−π* and parallel π−π* transitions, respectively, and a positive maximum at 192 nm assigned to the perpendicular π−π* transition.[26]

The fluorescence emission spectra are characterized by a single peak, maximal at 344 nm (Figure 4B), arising from the contributions of two tryptophan residues, one (Trp-135) located in the second α-helix of domain IB in a solvent-exposed hydrophobic pocket close to the protein surface (λ_{max} = 348 nm), the other (Trp-214) buried deep in BSA's interior within the hydrophobic pocket of domain IIA (λ_{max} = 332 nm) participating in a hydrophobic packing interaction at the IIA−IIIA interface.[27−31]

CD spectra of mAb (Figure 4D) have the character of an antiparallel β-sheet-rich immunoglobulin, with a positive maximum at 202 nm assigned to the π−π* transition, a negative maximum at 217 nm from the n−π* transition, and a distinctive broad shoulder near 230 nm that has previously been ascribed to contributions from aromatic side chains.[32,33] The intrinsic fluorescence spectra (Figure 4F) have a λ_{max} at 338 nm, resulting from the predominant contribution of tryptophan. The corresponding absorbance spectra of BSA and mAb (Figure 4, parts B and E) are both typical of absorption from the peptide backbone, with a peak at 190 nm and shoulder at 220 nm.

With the ht-caCD/F system's strong optical performance and consistent automated sample delivery confirmed, we next explored the ht-caCD/F systems potential as a PAT tool in bioprocess development in two industrially relevant case studies, namely, (i) monitoring the unfolding of BSA (a well-characterized and frequently employed model protein) and a therapeutic mAb under increasing concentrations of the chaotropic agent urea and (ii) testing the stability of a therapeutic mAb across a range of pH used in downstream purification.

Case Study 1: Denaturation by Urea. Chaotropic agents such as urea or guanidine hydrochloride are frequently used to probe the unfolding events of biological molecules and are widely employed in industrial bioprocessing settings, e.g., for the resolubilization of inclusion bodies or as stabilizing additives in elution buffers.[34,35] Here, we employed the automated ht-caCD/F system to interrogate structural changes induced in BSA and mAb following 1 h of exposure to various concentrations (0−8 M) of urea.

The addition of low concentrations of urea (1 and 2 M) to BSA resulted in no observable change to its CD spectrum (Figure 5A). With increasing urea concentration beyond 3 M, however, significant loss in α-helical content occurred; the far-UV CD spectrum (Figure 5, parts A and B) became progressively less negative, and the magnitude of the 222 nm maximum diminished in roughly linear fashion with increase in urea concentration between 2 and 7 M (Figure 5B). At the highest urea concentration employed (8 M), the 222 nm maximum observed in the native BSA spectrum was no longer visible, but the negative shoulder between 215 and 230 nm implies that BSA, though denatured, is not completely unfolded, i.e., it exists in a denatured constrained state devoid of long-range order.[36−38]

The fluorescence emission spectra corresponding to the Figure 5A CD data show urea concentration-dependent quenching of tryptophan fluorescence (Figure 5C), with little quenching observed at lower concentrations and strong quenching above 3 M urea, with normalized fluorescence intensity falling to ca. 50% at 7 M urea (Figure 5D). The fluorescence wavelength maximum, λ_{max} (Figure 5D), undergoes gradual blue (hypsochromic) shifting over the 0−5 M urea concentration range (falling from 344.8 to 340.6 nm) followed by strong red (bathochromic) shifting between 5 and 8 M urea (λ_{max} reaching 349.1 nm). These results are in strong agreement with urea-dependent hypsochromic and bathochromic shifts in BSA's fluorescence emission spectrum reported previously,[30] and likely reflect a two-stage rearrangement of the protein's packing structure. In the first stage, we envisage limited unfolding by low concentrations of the chaotrope (1−5 M urea) creates a more hydrophobic environment around Trp-214, resulting in the observed hypsochromic shift, and in the second, high chaotrope concentrations (6−8 M urea) induce extensive unfolding and exposure of tryptophan residues to a polar solvent environment, and a concomitant bathochromic shift.

The unfolding of mAb in urea differed markedly from that exhibited by BSA. With increasing urea concentration the mAb showed little conformational change until 6 M urea (Figure 6). The CD spectra showed most variance at low wavelengths,

DOI: 10.1021/acs.analchem.9b03259
Anal. Chem. 2019, 91, 13794−13802

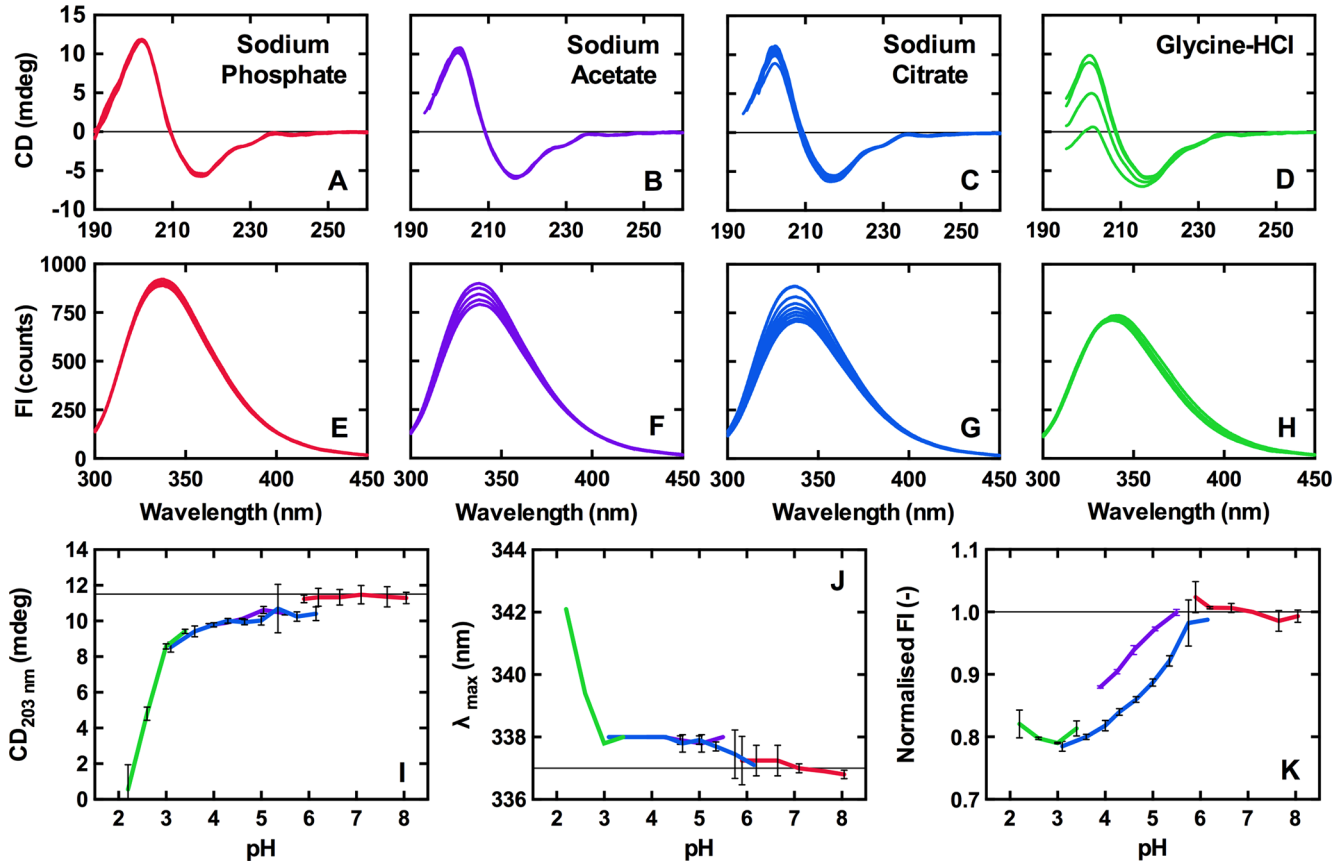

Figure 7. Case study 2: monoclonal antibody stability testing. Twenty-four different buffers spanning the pH range of 2.2−8.05 were tested with mAb at a final concentration of 0.20 mg/mL, i.e., 20 mM sodium phosphate (pH 8.05, 7.65, 7.10, 6.60, 6.20, and 5.85), sodium acetate (pH 5.50, 5.05, 4.60, 4.25, and 3.90), sodium citrate (pH 6.15, 5.75, 5.35, 5.00, 4.65, 4.30, 4.00, 3.60, and 3.10), and glycine−hydrochloric acid (pH 3.40, 3.00, 2.60, and 2.20). Triple air-segmented delivery was employed to inject 40 μL samples. Each sample was loaded twice, and the obtained spectra were averaged. (A−D) CD spectra were collected in continuous scan mode with the following parameters: bandwidth = 2 nm; scan speed = 100 nm/min; DIT = 1s; averaging over four accumulated scans per sample. (E−H) Fluorescence spectra were averaged over five accumulated scans per sample (DIT = 4 s). (I) CD_{203nm} vs pH. (J) λ_{max} vs pH. (K) Normalized fluorescence intensity vs pH. Error bars correspond to the standard deviation of two independent measurements.

which were largely obscured by the cutoff limit arising from urea absorbance at ∼210 nm (Figure 6, parts A and B). Loss of β-sheet structure was reported at 213 nm in the presence of ≥6 M urea, and at 8 M a small change at 238 nm was also observed. A considerable bathochromic shift of the fluorescence signal at 7−8 M urea indicates extensive unfolding of protein structure at high chaotrope concentrations, reaching 346.3 nm at 8 M cf. 337.6 in native state (Figure 6D). This red shift coincided with a dramatic increase in fluorescence intensity (reaching twice the native emission at 8 M urea). Unlike BSA, the intrinsic fluorescence emission of the native state was more quenched than in the denatured state, which is typical of immunoglobulin domains due to the close proximity of tryptophan residues to disulfide bonds in the folded conformation.[39,40]

Case Study 2: mAb Stability Testing. Protein A chromatography is the most widely used initial capture step in antibody purification in industry. The high affinity of Protein A for the Fc region of immunoglobulin facilitates >95% purification in a single processing step. However, low-pH elution buffers are required to break the protein's interaction with resin, often ranging from pH 2.5 to 4.[41,42] Furthermore, in pharmaceutical operations, mAbs are incubated following elution at low pH for long periods of time for viral inactivation.[5] The acidic conditions used in mAb downstream processing are often considered to contribute to the deterioration in product integrity.[43] In particular, Protein A chromatography is frequently associated with increased inactivation rates due to aggregation.[35,44] Thus, it is important to understand the acid tolerance of mAb products on a case-by-case basis.

This work has employed automated ht-caCD/F to interrogate the structural transitions of mAb (0.20 mg/mL final concentration) formulated in buffers commonly employed during the various stages (loading, washing, elution, viral hold) of Protein A affinity chromatography (Figure 7). Twenty-four different buffers spanning the pH range of 2.2−8.05 were tested (i.e., sodium phosphate, pH 5.85−8.05; sodium acetate, pH 3.9−5.5; sodium citrate, pH 3.1−6.15; glycine−hydrochloric acid, pH 2.2−3.4), and these were employed at 20 mM so as to maintain low background absorption in the far-UV region.

At near-neutral pH values (encountered during loading and washing phases) the CD (Figure 7A) and fluorescence (Figure 7B) spectra (Figure 7I−K) indicate little variation in mAb structure between pH 8 and 6. With further reduction in pH from 6 to 3, a slight gradual drop in ellipticity at 203 nm from ∼10 to 8.5 mdeg (Figure 7I) is paralleled by a 1 nm red shift in

DOI: 10.1021/acs.analchem.9b03259
Anal. Chem. 2019, 91, 13794−13802

λ_{max} (from 337 to 338 nm; Figure 7J) and marked drop (>20%; Figure 7K) in fluorescence intensity. The stronger fluorescence quenching of aromatic residues within the mAb by citrate cf. acetate (Figure 7, parts F, G, and K) is likely due to preferential accumulation of quenching citrate ions near the mAb's surface.[43−46]

More significant perturbations to mAb structure are observed as the pH is reduced yet further from ∼3 to 2.2, with CD revealing severe loss of β sheet structure (CD_{203nm} falling from >8 mdeg to <0.5 mdeg; Figure 7, parts D and I) and fluorescence spectra showing strong red shifting of λ_{max} (from 338 to 342 nm; Figure 7, parts H and J), but no further quenching (Figure 7, parts H and K). The spectral changes recorded here are in keeping with two phase structural rearrangements previously observed for immunoglobins exposed to low pH,[47,48] with onset of unfolding occurring below pH 6 and severe distortion of structure evident below pH 3.

CONCLUSION

CD and fluorescence spectroscopy provide valuable insights into the intricate unfolding events of proteins. The automation of a system that integrates an automated loading robot and low-volume capillary flow cell with these orthogonal spectroscopic techniques has been described and evaluated with respect to (i) loading method, (ii) data quality, and (iii) sample requirements. We found that air-segmented delivery of samples was the best loading method, and the use of a fixed-position quartz capillary flow cell afforded consistently high-quality spectra. Further, we showed that reproducible and high transfer efficiency loading could be achieved using sample volumes as low as 40 μL. Thus, this system provides a number of benefits that include eliminating manual sample loading and cleaning procedures, reducing sample requirements by up to 5-fold, and increasing productive machine time for prolonged, unattended running periods. In an industrial or research setting, these advantages could translate into important time and cost savings.

The presented case studies demonstrated the utility of ht-caCD/F for rapidly evaluating the distinct unfolding patterns of secondary and tertiary elements of protein, delivering precisely the results expected had CD and fluorescence measurement been conducted in conventional manner. Under increasing concentrations of urea, unfolding of BSA was seen to occur at >2 M via an intermediate state at 5 M urea, whereas mAb retained it structure up to >6 M urea. It is noteworthy that operation of the ht-caCD/F system was unperturbed by the high viscosity of concentrated (8 M) urea solutions. In a process development application, unfolding of an IgG1 in various low-pH buffers was shown to occur via a two-stage unfolding sequence, with partial unfolding occurring between pH 6 and 3 and severe unfolding below pH 3. Quickly gathering such information can be invaluable for informing the choice of appropriate processing or formulation conditions to reduce the risk of costly downstream failure. In an industrial biomanufacturing setting, we envisage further adaption of the described system to collect structural data from proteins as they elute off chromatography columns. While chiral detection of optically active compounds in HPLC systems has hitherto proven useful for the detection of biologically significant small molecules,[20,21] the combination of new, sensitive CD and fluorescence detectors with capillary flow paths presents a promising opportunity to monitor conformational changes of eluted proteins and overcome the sensitivity issues reported in previous endeavors.[49]

ASSOCIATED CONTENT

Supporting Information

The Supporting Information is available free of charge on the ACS Publications website at DOI: 10.1021/acs.analchem.9b03259.

Diagram illustrating the loading of triple-segmented sample, autosampler settings for air-segmented injection, circuit board diagram for controlling modular components with a Raspberry Pi B+, HPLC pump profiles, Python (version 3.5) program used to control Raspberry Pi B+, and CD_{222nm} vs time plots for sample contained between various segmenting bubble volumes (PDF)

AUTHOR INFORMATION

Corresponding Author

*Phone: +44 0 121 414 5278. E-mail: o.r.t.thomas@bham.ac.uk.

ORCID

Owen R. T. Thomas: 0000-0001-8253-365X

Present Address

⊥C.M.-K.: Oxford Biomedica, Windrush Court, Transport Way, Oxford OX4 6LT, U.K. E-mail: c.moore-kelly@oxb.com.

Author Contributions

The experimental work was performed by C.M.-K. and supervised by T.R.D. and O.R.T.T. C.M.-K. and O.R.T.T. wrote the manuscript with valuable contributions from A.R. and T.R.D. All authors have given approval to the final version of the manuscript.

Notes

The authors declare no competing financial interest.

ACKNOWLEDGMENTS

This work was supported by the EPSRC Centre for Doctoral Training in Formulation Engineering (Grant No. EP/L015153/1) and Pall Biotech.

REFERENCES

(1) Gronemeyer, P.; Ditz, R.; Strube, J. *Bioengineering* **2014**, *1*, 188−212.

(2) Orphanou, C.; Gervais, D. *J. Chem. Technol. Biotechnol.* **2018**, *93*, 2477−2485.

(3) Tavakoli-Keshe, R.; Phillips, J. J.; Turner, R.; Bracewell, D. G. *J. Pharm. Sci.* **2014**, *103*, 437−444.

(4) Sharma, B. *Biotechnol. Adv.* **2007**, *25*, 325−331.

(5) Vázquez-Rey, M.; Lang, D. A. *Biotechnol. Bioeng.* **2011**, *108*, 1494−1508.

(6) Pharmaceutical cGMPs for the 21st century—A risk based approach: Final report, September 2004. https://www.fda.gov/media/77391/download (accessed July 17, 2019).

(7) Guidance for industry: PAT—A framework for innovative pharmaceutical development, manufacturing and quality assurance, September 2004. https://www.fda.gov/media/71012/download (accessed July 17, 2019).

(8) Hinz, D. C. *Anal. Bioanal. Chem.* **2006**, *384*, 1036−1042.

(9) Scott, B.; Wilcock, A. *PDA J. Pharm. Sci. Technol.* **2006**, *60*, 17−53.

(10) Rathore, A. S.; Kapoor, G. *J. Chem. Technol. Biotechnol.* **2015**, *90*, 228−236.

(11) Kelly, S. M.; Jess, T. J.; Price, N. C. *Biochim. Biophys. Acta, Proteins Proteomics* **2005**, *1751*, 119−139.

DOI: 10.1021/acs.analchem.9b03259
Anal. Chem. 2019, 91, 13794−13802

(12) Lakowicz, J. R. *Principles of Fluorescence Spectroscopy*; Springer: New York, 2006.
(13) Vivian, J. T.; Callis, P. R. *Biophys. J.* **2001**, *80*, 2093−2109.
(14) Aucamp, J. P.; Cosme, A. M.; Lye, G. J.; Dalby, P. A. *Biotechnol. Bioeng.* **2005**, *89*, 599−607.
(15) Royer, C. A. *Chem. Rev.* **2006**, *106*, 1769−1784.
(16) Gaudet, M.; Remtulla, N.; Jackson, S. E.; Main, E. R. G.; Bracewell, D. G.; Aeppli, G.; Dalby, P. *Protein Sci.* **2010**, *19*, 1544−1554.
(17) Sagar, D. M.; Aoudjane, S.; Gaudet, M.; Aeppli, G.; Dalby, P. A. *Sci. Rep.* **2013**, *3*, 2130.
(18) Maddux, N. R.; Rosen, I. T.; Hu, L.; Olsen, C. M.; Volkin, D. B.; Middaugh, C. R. *J. Pharm. Sci.* **2012**, *101*, 2017−2024.
(19) Fiedler, S.; Cole, L.; Keller, S. *Anal. Chem.* **2013**, *85*, 1868−1872.
(20) Synovec, R. E.; Yeung, E. S. *Anal. Chem.* **1985**, *57*, 2606−2610.
(21) Synovec, R. E.; Yeung, E. S. *J. Chromatogr.* **1986**, *368*, 85−93.
(22) Waldron, D. E.; Marrington, R.; Grant, M. C.; Hicks, M. R.; Rodger, A. *Chirality* **2010**, *22*, E136−E141.
(23) Miles, A. J.; Wien, F.; Lees, J. G.; Rodger, A.; Janes, R. W.; Wallace, B. A. *Spectroscopy* **2003**, *17*, 653−661.
(24) Sreerama, N.; Woody, R. W. *Anal. Biochem.* **1993**, *209*, 32−44.
(25) Compton, L. A.; Johnson, W. C., Jr. *Anal. Biochem.* **1986**, *155*, 155−167.
(26) Holzwarth, G.; Doty, P. *J. Am. Chem. Soc.* **1965**, *87*, 218−228.
(27) Burstein, E. A.; Vedenkina, N. S.; Ivkova, M. N. *Photochem. Photobiol.* **1973**, *18*, 263−279.
(28) Chadborn, N.; Bryant, J.; Bain, A. J.; O'Shea, P. *Biophys. J.* **1999**, *76*, 2198−2207.
(29) Carter, D. C.; Ho, J. X. *Adv. Protein Chem.* **1994**, *45*, 153−203.
(30) Kumaran, R.; Ramamurthy, P. *J. Fluoresc.* **2011**, *21*, 1499−1508.
(31) Majorek, K. A.; Porebski, P. J.; Dayal, A.; Zimmerman, M. D.; Jablonska, K.; Stewart, A. J.; Chruszcz, M.; Minor, W. *Mol. Immunol.* **2012**, *52*, 174−182.
(32) Cathou, R. E.; Kulczycki, A.; Haber, E. *Biochemistry* **1968**, *7*, 3958−3964.
(33) Vermeer, A. W.; Bremer, M. G.; Norde, W. *Biochim. Biophys. Acta, Gen. Subj.* **1998**, *1425*, 1−12.
(34) Singh, A.; Upadhyay, V.; Upadhyay, A. K.; Singh, S. M.; Panda, A. K. *Microb. Cell Fact.* **2015**, *14*, 41.
(35) Shukla, A. A.; Gupta, P.; Han, X. *J. Chromatogr. A* **2007**, *1171*, 22−28.
(36) Fasman, G. D.; Hoving, H.; Timasheff, S. N. *Biochemistry* **1970**, *9*, 3316−3324.
(37) Barnes, K. P.; Warren, J. R.; Gordon, J. A. *J. Biol. Chem.* **1972**, *247*, 1708−1712.
(38) Shortle, D.; Ackerman, M. S. *Science* **2001**, *293*, 487−489.
(39) Cowgill, R. W. *Arch. Biochem. Biophys.* **1963**, *100*, 36−44.
(40) Vinci, F.; Catharino, S.; Frey, S.; Buchner, J.; Marino, G.; Pucci, P.; Ruoppolo, M. *J. Biol. Chem.* **2004**, *279*, 15059−15066.
(41) Fahrner, R. L.; Knudsen, H. L.; Basey, C. D.; Galan, W.; Feuerhelm, D.; Vanderlaan, M.; Blank, G. S. *Biotechnol. Genet. Eng. Rev.* **2001**, *18*, 301−327.
(42) Liu, H. F.; Ma, J.; Winter, C.; Bayer, R. *MAbs* **2010**, *2*, 480−499.
(43) Roberts, C. J. *Trends Biotechnol.* **2014**, *32*, 372−380.
(44) Mazzer, A. R.; Perraud, X.; Halley, J.; O'Hara, J.; Bracewell, D. G. *J. Chromatogr. A* **2015**, *1415*, 83−90.
(45) Barnett, G. V.; Razinkov, V. I.; Kerwin, B. A.; Laue, T. M.; Woodka, A. H.; Butler, P. D.; Perevozchikova, T.; Roberts, C. J. *J. Phys. Chem. B* **2015**, *119*, 5793−5804.
(46) Barnett, G. V.; Razinkov, V. I.; Kerwin, B. A.; Hillsley, A.; Roberts, C. J. *J. Pharm. Sci.* **2016**, *105*, 1066−1073.
(47) Buchner, J.; Renner, M.; Lilie, H.; Hinz, H. J.; Jaenicke, R.; Kiefhaber, T.; Rudolph, R. *Biochemistry* **1991**, *30*, 6922−6929.
(48) Vermeer, A. W.; Norde, W. *Biophys. J.* **2000**, *78*, 394−404.
(49) Luykx, D. M. A. M.; Goerdayal, S. S.; Dingemanse, P. J.; Jiskoot, W.; Jongen, P. M. J. M. *J. Chromatogr. B: Anal. Technol. Biomed. Life Sci.* **2005**, *821*, 45−52.

DOI: 10.1021/acs.analchem.9b03259
Anal. Chem. 2019, 91, 13794−13802